Effects of the Loading Direction on High Strain Rate Behavior of Woven Graphite/Epoxy Composites

Fatih Turan
Mechanical Engineering Department, Istanbul University
E-mail: fatihturan@istanbul.edu.tr

Mohammad R. Allazadeh
Institute of Mechanical Engineering, University of Pannonia
Veszprem, H-8200, Hungary
E-mail: mrallazadeh@yahoo.com

Sylvanus N. Wosu
Mechanical Engineering and Materials Science Department
University of Pittsburgh, Pittsburgh, PA 15261, USA
E-mail: snn2@pitt.edu

Received: September 19, 2011 Accepted: October 6, 2011 Published: Apri1 1, 2012
doi:10.5539/jmsr.v1n2p69 URL: http://dx.doi.org/10.5539/jmsr.v1n2p69

Abstract

Effects of the loading direction on high strain rate behavior of cylindrical woven graphite/epoxy composites are presented. Compressive split Hopkinson pressure bar (SHPB) was used for high strain rate experiments. Cylindrical specimens were loaded diametrically and transversely at the impact energies of 67 J, 163 J, and 263 J. Micro Laser Raman spectroscopy and scanning electron microscopy (SEM) were used for surface characterization. It is observed that diametrically loaded specimens show permanent plastic deformation with high ductility resulting in a catastrophic failure while transversely loaded specimens exhibit viscoplastic deformation with some recoverable damage. As a result of this, Raman peak shifted to higher values for the diametrically loaded fibers whereas almost no change was observed in the Raman shift of transversely loaded fibers.

Keywords: High strain rate, P-SHPB, Raman spectrum, Impact load, Woven graphite epoxy composite, Longitudinal loading, Diametrical loading

1. Introduction

Composite materials have been widely used in many applications in which high strength to weight ratio is required such as aircraft structures, space shuttles, armored vehicles, and automobiles (Daniel & Ishai, 1994). In some cases such as automobile accidents, bird strikes on aircraft structures, and ballistic impact loading on armored vehicles, these composites are exposed to high strain rate loading. The impact loading in these cases may be varied in loading direction and therefore, it is vital to understand the effect of the loading direction on high strain rate behavior of woven graphite/epoxy composites. The widely used technique for the determination of high strain rate behavior of composites is split Hopkinson pressure bar apparatus which works based on one dimensional wave propagation theory in elastic bars.

Many studies were conducted to understand high strain rate behavior of unidirectional and cross – ply carbon composites (Hsiao & Daniel, 1996; Hsiao, Daniel & Cordes, 1998, 1999; Li & Lambros, 1999; Vinson & Woldesenbet, 2001; Hosur, *et al.*, 2001) and woven fabric carbon composites (Hou & Ruiz, 2000; Hosur, *et al.*, 2003, 2004a, 2004b) under compressive loading. It was generally observed that the compressive strength and modulus increase with increasing strain rate. N. K. Naik *et al.* (Naik & Venkateswara, 2008) concluded that

compressive strength and failure strain increase with increasing strain rate in thickness directions compared with those along warp and fill directions and compressive modulus is lower along thickness directions compared with those along warp and fill directions. I. W. Hall and M. Guden (Hall & Guden, 2001) carried out research to determine the mechanical properties and failure mechanisms of unidirectional reinforced graphite/epoxy composites using a compression Split Hopkinson Pressure Bar. Their results showed that there is a strong rate dependency on the strength properties in the transverse direction but no similar dependence is observed longitudinally.

Raman spectroscopy is an analytical technique that yields information about the molecular structure of materials based on the observation of scattered light spectra. Raman spectroscopy is sensitive to molecular interactions in materials such as Kevlar, graphite, and carbon used as reinforcement in composites (Galiotis & Batchelder, 1998; Young, 1997; Sato, Tatsuda & Kurauchi, 1992). These studies have also shown that Raman spectroscopy is applicable for strain measurement. The Raman peak of a molecule is dependent upon its molecular geometry that depends on the externally applied load due to changes in the molecular geometry. The peak frequency shifts to a lower value under tension due to increasing bond length between atoms and to a higher value under compression due to decreasing bond length between atoms and therefore the level of stress or strain of the fiber through the shift of the peak frequency can be measured. Raman spectrum plots the shift in Raman spectrum in cm^{-1} versus Raman intensity in an arbitrary unit (a. u.). This relationship between vibrational frequency and applied load can be useful to obtain stress - strain distribution of the fibers. Once stress and strain distribution is found, then one can measure the failure mechanisms of the fibers embedded in the composites since each failure mechanism occurs at different energy level.

The high strain rate behavior of diametrically and transversely loaded cylindrical woven graphite composites has not been compared yet. Thus, the objective of the present study is to determine the high strain rate behavior of diametrically and transversely loaded cylindrical woven graphite/epoxy composites and to characterize the surface morphology of damaged specimens subjected to the impact loading using micro Raman Spectroscopy and SEM.

2. Experimental Technique

The composite materials used in this study are graphite/epoxy composites and fabricated by VARIM process using plain weave T300B – 40B – 3K – Toray carbon fabric as a reinforcement material and SC – 14 epoxy resin as a matrix material. The thicknesses of the composite materials are 12 ply (2.87 mm), and 16 ply (3.55 mm) with a diameter of 25.4 mm. Figure 1 shows the schematic of the plain weave ply.

A SHPB was used for high strain rate testing. The compression Hopkinson bar apparatus consists of incident, transmitter, and striker bars (300 Maraging AMS 6514 steel). The incident and transmitter bars are 3.66 m and the striker bar is 0.61 m in length while all bars are 0.0254 m in diameter. Also a retracting rod attached to the striker bar is used to pull back the striker bar to desired ram length then the striker bar has a kinetic energy according to that ram length. During the test, the specimen is sandwiched between the incident and transmitted bars. Typical setup of SHPB is shown schematically in Figure 2.

When the striker bar hits the incident bar, a compressive stress/strain pulse is produced on the impact end of the incident bar. This compressive pulse traveling through the incident bar reflects at the free surface as a tensile pulse and returns to the impact face. Thus, the pulse in the incident pressure bar is twice the length of the striker bar. This pulse (incident pulse) travels through the incident bar toward the incident bar – specimen interface and is recorded by the strain gage located in the midpoint of the incident bar after 395 microseconds. The incident pulse reaches the interface of the incident bar and specimen at 790 μs where some portion of it is reflected back to the incident bar as a tensile (reflected) pulse and some portion is transmitted to the transmitter bar as a compressive pulse. It should be noted that the reflected pulse starts a little earlier than the transmitted pulse. This short delaying time occurs due to the finite thickness of the specimen. During the period of stress wave propagation through the specimen, the specimen undergoes deformation until its dynamic limit is reached. The relative magnitudes of these pulses depend on the physical properties of the specimen. The properties of the bar materials such as density, bar wave velocity, and diameter and the specimen dimensions are known prior to the data analysis from a SHPB test. From the signals obtained by the strain gages and using one dimensional wave propagation theory, the analytical relations to calculate strain, strain rate, and stress as a function of time in the specimen in SHPB testing can be calculated, respectively, as next (Allazadeh & Wosu, 2011a),

$$\varepsilon_s(t) = -\frac{2C_0}{L_0}\int_0^t [\varepsilon_r(t)]dt \quad (1)$$

$$\dot{\varepsilon_s}(t) = -\frac{2C_0}{L_0}\varepsilon_r(t) \tag{2}$$

$$\sigma_s(t) = \frac{A_b E_0 \varepsilon_t(t)}{A_s} \tag{3}$$

where C_o is the elastic wave velocity in the bars, L_o is the specimen initial length, A_b is the cross sectional area of the bars, A_s is the cross sectional area of the specimen, E_o is the Young's modulus of the bars, ε_t is the transmitted strain pulse, ε_r is the reflected strain pulse, and *t* is the time duration. Figures 3 and 4 shows typical loading configurations for specimens loaded transversely and diametrically, respectively. The energy absorption can be calculated as (Allazadeh & Wosu, 2011b):

$$E_A(t) = \frac{A_S C_o}{E_o}\int_0^t [\sigma_i^2(t) - \sigma_r^2(t) - \sigma_t^2(t)]\, dt \tag{4}$$

Subscript *i*, *r* and t of σ in equation 4 indicate incident, reflected and transmitted stress waves, respectively. The purpose of the system calibration is to obtain a relationship between the compressed pressure applied to the system and the striker velocity delivered to the incident bar and the energy transferred to the incident bar. A photo gate detector and a 0.023 m flag were used to measure the duration of the blocking time in photo gate detectors. The flag was attached to the end of the striker rod (attached to the striker bar end). At the release of compressed air in the striker bar chamber, the striker bar/rod assembly moves toward the incident bar and the flag blocks the infrared beam in photo gate detectors just before the impact. The blocking time is obtained from a software program connected to the photo gate detectors (Data Studio). The blocking time measured in photo gate detectors divided by the length of the flag gives the striker bar impact velocity as photo gate detector was positioned to measure the striker impact velocity just before the impact with the incident bar. The striker bar impact energy transferred to the system is equal to the initial kinetic energy of the impact bar and can be expressed by (Nwosu, 1996),

$$E_i = \frac{1}{2} m_s {V_i}^2 \tag{5}$$

where m_s is the mass of the striker bar and V_i is the impact bar velocity. Finally, calibration curve can be obtained plotting striker velocity versus applied pressure and corresponding energy versus applied pressure data. Figure 5 gives the calibration curves showing there is a nonlinear relationship between the striker velocity and applied pressure.

3. Results and Discussion

3.1 Effect of the Loading Direction on the Energy Absorbed

Figure 6 shows the effect of loading direction on the energy absorbed for 12 ply specimens loaded at 67 J and 163 J impact energies. In the case of transverse loading, reflected wave is negligible allowing almost all incident wave energy to be transmitted to the transmitter bar. No tensile-release wave to cause any significant surface damage since reflected wave is a direct measure of surface damage. However, in the case of diametrical loading, reflected wave is quite significant and consequently the transmitted wave is almost zero indicating that there is a significant transfer of the initial impact energy for damage process as shown in Figure 7. The transversely loaded specimen remained mostly in compression with no appreciable tensile release wave. Due to the greater reflected wave the energy or stress released in tension after 300 microseconds of damage event is greater with diametrical loading than with transverse loading as shown Figure 8. The transversely loaded specimen continued to linearly absorb energy during most of the damage process with no visible surface damage. These combined observations clearly show that a significant amount of impact energy is absorbed in the case of transverse loading compared to diametrical loading. This shows that the amount of energy spent in the permanent damage process is small in transversely loaded case; only friction and heating consume the applied impact energy for transverse loading case although visible permanent damage with significant energy consumption occurs in the specimens subjected to the diametrical loading.

3.2 Effect of the Loading Direction on Stress – Strain Behavior

The area considered in the stress calculation for the diametrical loading case can be expressed as $A_i = t \times x_i$, where t is the thickness of the specimen which is constant and x_i is the contact length which varies with respect to the cross sectional area of the specimen in the loading direction as shown in Figure 9. The value of x

was chosen as 3.80 mm which is close to the contact point and used to estimate maximum stress in the specimen. In the case of transverse loading, the area considered in the calculation is the surface area of the cylindrical specimens.

The nature of the stress – strain curves of both the diametrically and transversely specimens in Figure 10 shows that the specimens subjected to transverse loading exhibit viscoplastic deformation with no visible damage while the specimens subjected to the diametrical loading exhibit completely plastic deformation with visible damage as shown in Figure 11 and 12. The nature of the boundary condition in the case of diametrical loading gives rise to plastic deformation in the region of the contact surface (see Figure 11) due to the stress concentration in the specimen as shown in Figure 9. Stress is highly localized at the contact surface and therefore stress concentration has its highest value at the contact point. This means that small portions of the specimen where the highly localized stresses occur absorb an excessive amount of energy before the main portion of the specimen can be stressed appreciably. As a result, the small portion where the highly localized stress occurs is likely to be stressed above the yield stress of the material. Hence, the peak plastic deformation is observed in the contact surface of the specimen (see Figure 11) while main portion of the specimen is in overall integrity (see Figure 12).

3.3 Effect of Loading Direction on Strain Rate – Strain Behavior

Figure 13 shows the effect of loading direction on strain rate – strain behavior for the 12 ply specimens at same impact energy. High strain rate is observed in transversely loaded specimens compared to the substantially low strain rate for diametrically loaded specimens despite the visible damage. This behavior is due to the fact that in the transverse loading, the fibers are expected to mainly flex with load perpendicular to the fiber direction. The specimens have significantly smaller initial length and sandwiched between two bars that prevented fibers from being flexed or deformed. However, longer initial length can make flexing and deformation easier for the fibers in diametrically loaded specimens where the load is in the direction of the fiber. The flat region for the diametrical loading case shows strain remained constant for reasonable time for damage to occur corresponding resulting in maximum plastic deformation and damage accumulation. The region of constant strain rate with time is missing in the transverse loading case. Figure 13 shows that the strain rate in transverse loading increased to a maximum and decreased to zero because the amplitude of the incident pulse did not produce sufficient stress to further deform the materials. With such instability due to large variation of strain rate no significant plastic deformation occurs in this case.

4. Surface Characterization

Surface characterization of the specimens by Raman spectroscopy was accomplished by running three trials for each energy level and loading condition (diametrically and transversely). The Raman shifts obtained from three trials were averaged and plotted as average Raman shift versus impact energy with standard deviations for these average values. Analysis of the results is shown the sections below:

4.1 Raman Spectrum and SEM Images of Transversely Loaded Specimens

Figure 14 shows the typical Raman spectrum of 16 ply transversely loaded specimens. It is very clear from this result that the intensity of Raman peak on the average increases with impact energy or incident compressive stress. Figure 15 gives the relationship between Raman shift and impact energy for transversely loaded 16 ply graphite/epoxy composites and shows that the Raman shift decreases slightly with applied impact energy. Figure 16 shows the SEM images of 16 ply transversely loaded specimens at various impact energies. Although Figure 12 shows no visible surface damage for transverse loading, the SEM results show that fiber breakages and fiber/matrix detachment for the transversely loaded occurs in the different regions below the composite. It should also be noted that the failure is only at the top layer at 67 J, although the number of the layer in which failure occurs increases with increasing applied energy.

4.2 Raman Spectrum and SEM Images of Diametrically Loaded Specimens

Figure 17 shows the typical Raman spectrum of diametrically loaded 16 ply specimens as an average. Unlike in the case of transverse loading, the intensity of Raman peak on the average also decreases with impact energy or incident compressive stress. Figure 18 gives the average relationship between Raman shift and impact energy for diametrically loaded 16 ply graphite/epoxy composites and shows that the Raman shift increases non-linearly with applied impact energy. The Raman shift of the damaged specimens is higher than that of the undamaged specimens as opposed to the transverse loading case where the Raman of the undamaged is higher than the damaged specimen. It is expected because at the contact surface, fibers of the diametrically loaded specimens are exposed to very intense impact loading absorbing significant amount of initial energy. This results in shorter

bond length between the neighboring atoms and that allows higher Raman shift. However, the increase in the Raman shift for the diametrically loaded specimens is not proportional to the increasing applied impact energy due to the fact that the each individual fiber might be exposed to different impact energy for the same impact energy or the beam spot might focus the fibers which are exposed to lower impact energy. It should also be noted that Raman peak of undamaged transversely and diametrically specimens for graphite are different as it is expected because different distance between neighboring atoms allows different atomic vibration.

Figure 19 shows the SEM images of 16 ply transversely loaded specimens at various impact energies. SEM images indicate that a catastrophic failure as a result of fiber/matrix detachment and fiber breakages, destroying the overall integrity of the impacted region for diametrically loaded specimens which can also be seen clearly in Figure 11.

5. Summary and Conclusion

High strain rate compression testing was carried out on diametrically and transversely loaded specimens at three different impact energies. Surface characterization of damaged specimens was achieved using Raman spectroscopy and SEM. Following conclusions were drawn from the study.

1). Most of the expendable energy for specimen damage returns to the system in the transverse loading case, with no visible incipient damage, while some portion of the energy absorption is consumed in the deformation process for the diametrical loading case.

2). Transversely loaded specimens exhibited viscoplastic deformation with some recoverable damage compared to diametrically loaded specimens that exhibited plastic deformation with no recoverable damage resulting in catastrophic failure in the specimens.

3). Specimen deformation was observed at a higher strain rate in the transversely loaded specimens than in the diametrically loaded specimens.

4). The Raman shift decreases slightly with applied impact energy (incident compressive stress) for transversely loading and increases with impact energy or incident compressive stress for diametrical loading.

5). Raman peak gives different values with respect to the fiber orientation. The dependence of Raman peak on the fiber orientation is due to the fact that Raman peak of graphite gives approximately 1610 cm^{-1} when the fibers are exposed to the laser beam transversely while it gives approximately 1580 cm^{-1} when the fibers are exposed to the laser beam diametrically (Compare the Raman peaks of diametrically and transversely loaded specimens for 0 J).

6). SEM images indicate that some micro – cracks on the top layers of transversely loaded specimens occur even though fiber/matrix detachment and matrix cracking are dominant in a large deformed region of the diametrically specimens.

7). The use of SEM and Raman analyses reveal specimen internal damage where visual observation alone was not able to show damage.

References

Allazadeh M. R., & Wosu Sylvanus N. (2011a). High Strain Rate Compressive Tests on Wood. *Strain, An international Journal for Experimental Mechanics, STRAIN-* (January 2011), http://dx.doi.org/10.1111/j.1475-1305.2010.00802.

Allazadeh M. R., & Wosu Sylvanus N. (2011b). High Strain Rate Compressive Tests on Woven Graphite Epoxy Composites. *Applied Composite Materials, 18*(4), 311-325, http://dx.doi.org/10.1007/s10443-010-9159-6.

Daniel, I. M., & Ishai, O. (1994). *Engineering mechanics of composite materials*. New York, NY: Oxford University Press.

Elleithy, R. H. (2000). The hierarchical structure and flexure behavior of woven carbon fiber epoxy composite. *Polymer Composites, 21*, 716-723. http://dx.doi.org/10.1002/pc.10225.

Galiotis, C., & Batchelder, D. N. (1998). Strain dependences of the first and second order raman spectra of carbon fibers. *Journal of Material Science Letters, 7*, 545-547. http://dx.doi.org/10.1007/BF01730722.

Hall, I. W., & Guden, M. (2001). High strain rate testing of a unidirectionaly reinforced graphite/epoxy composite. *Journal of Material Science Letters, 20*, 897-899. http://dx.doi.org/10.1023/A:1010968514339.

Hosur, M. V., Adya, M., Jeelani, S., Vaidya, U. K., & Dutta, P. K. (2004a). Experimental studies on the high strain rate compression response of woven graphite/epoxy composites at room and elevated temperatures. *J. Reinforced Plast. Compos., 23*, 491-514. http://dx.doi.org/10.1177/0731684404032019.

Hosur, M. V., Adya, M., Vaidya, U. K., Mayer, A., & Jeelani S. (2004b). Studies on the off-axis high strain rate compression loading of satin weave carbon/epoxy composites. *Composite Structures, 63*, 75-85. http://dx.doi.org/10.1016/S0263-8223(03)00134-X.

Hosur, M. V., Adya, M., Vaidya, U. K., Mayer, A., & Jeelani, S. (2003). Effect of stitching and weave architecture on the high strain rate compression response of affordable woven carbon/epoxy composites. *Composite Structures, 59*, 507-523.

Hosur, M. V., Alexander, J., Vaidya, U. K., & Jeelani S. (2001). High strain rate compression response of carbon/epoxy laminate composites. *Composite Structures, 52*, 405-417. http://dx.doi.org/10.1016/S0263-8223(01)00031-9.

Hou, J. P., & Ruiz, C. (2000). Measurement of the material properties of woven CFRP T300/914 at different strain rates. *Composites Science and Technology, 60*, 2829-2834. http://dx.doi.org/10.1016/S0266-3538(00)00151-2.

Hsiao, H. M., Daniel, I. M., & Cordes, R. D. (1998). Dynamic compressive behavior of thick composite materials. *Experimental Mechanics, 38*, 172-180. http://dx.doi.org/10.1007/BF02325740.

Hsiao, H. M., Daniel, I. M., & Cordes, R.D. (1999). Strain rate effects on the transverse compressive and shear behavior of unidirectional composites. *Journal of Composite Materials, 33*, 1620-1642. http://dx.doi.org/10.1177/002199839903301703.

Hsiao, H.M., & Daniel, I. M. (1996). Failure mechanisms in thick composites under compressive loading. *Composites, 27*, 543-552. http://dx.doi.org/10.1016/1359-8368(95)00010-0.

Li, Z., & Lambros, J. (1999). Determination of dynamic response of brittle composites by the split hopkinson pressure bars. *Compos. Science. Technology, 59*, 1097-1107. http://dx.doi.org/10.1016/S0266-3538(98)00152-3.

Naik, N. K., & Venkateswara, R. K. (2008). High strain rate behavior of woven fabric composites under compressive loading. *Materials Science and Engineering, A474*, 301-311. http://dx.doi.org/10.1016/j.msea.2007.05.032.

Nwosu S. N. (1996). Hopkinson bar perforation of Laminated graphite/ epoxy composite. USAFORS report WL-TR-96-3080, l-66.

Sato, N., Tatsuda, N., & Kurauchi, T. (1992) .Application of laser raman spectroscopy to the analysis of stress distribution of fibers in composites. *Journal of Material Science Letters, 11*, 365-366. http://dx.doi.org/10.1007/BF00729184.

Vinson, J.R., & Woldesenbet, E. (2001). Fiber orientation effects on high strain rate properties of graphite/epoxy composites. *Journal of Composite Materials, 35*, 509-521. http://dx.doi.org/10.1177/002199801772662136.

Young, R. J. (1997). Analysis of composites using raman and flourence microscopy-a review. *Journal of Microscopy, 185*, 199-205. http://dx.doi.org/10.1046/j.1365-2818.1997.d01-618.x.

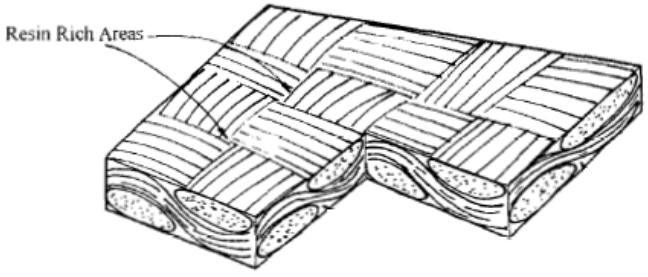

Figure 1. Schematic representation of the plain weave ply (Elleithy, 2000)

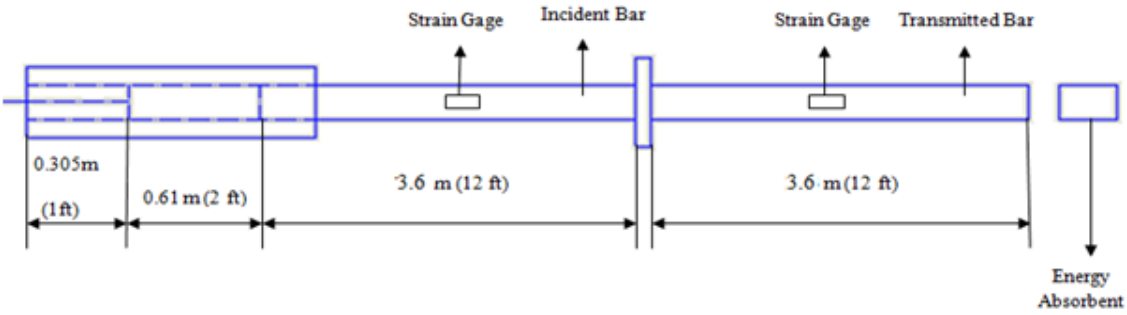

Figure 2. Schematic of the Hopkinson bar

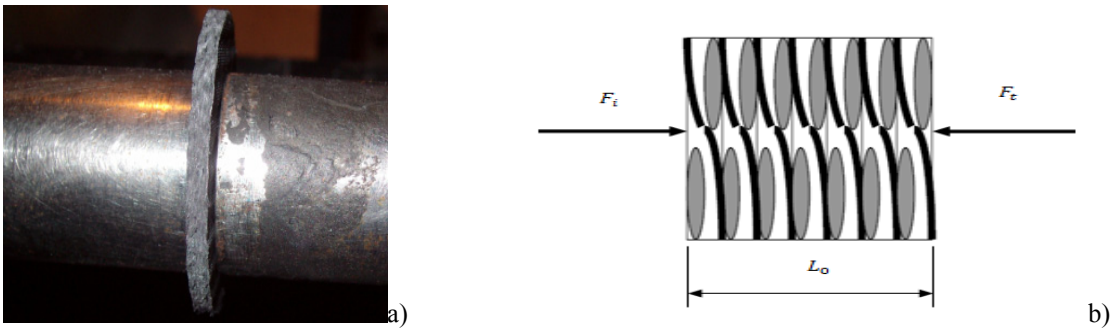

a) b)

Figure 3. Transverse loading configurations: a) transversely loaded specimen sandwiched between bars and b) loading direction that fibers are exposed to

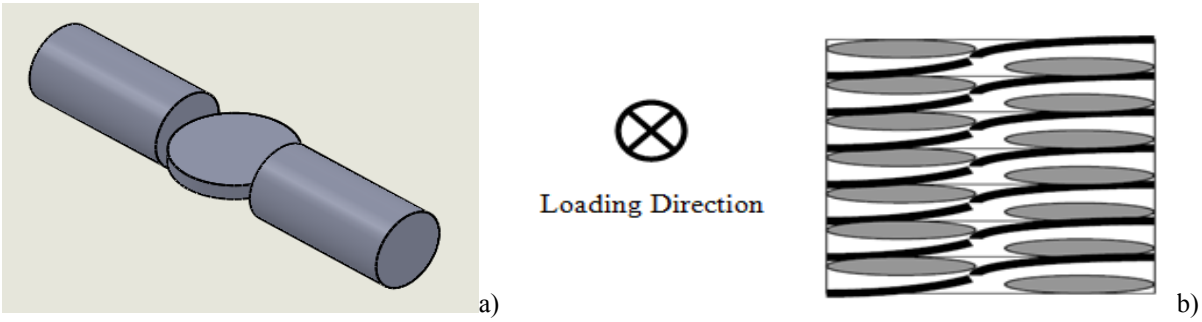

a) b)

Figure 4. Diametrical loading configuration: a) schematic view of diametrically loaded specimen by SHPB, b) loading direction applied to the fibers of the specimen

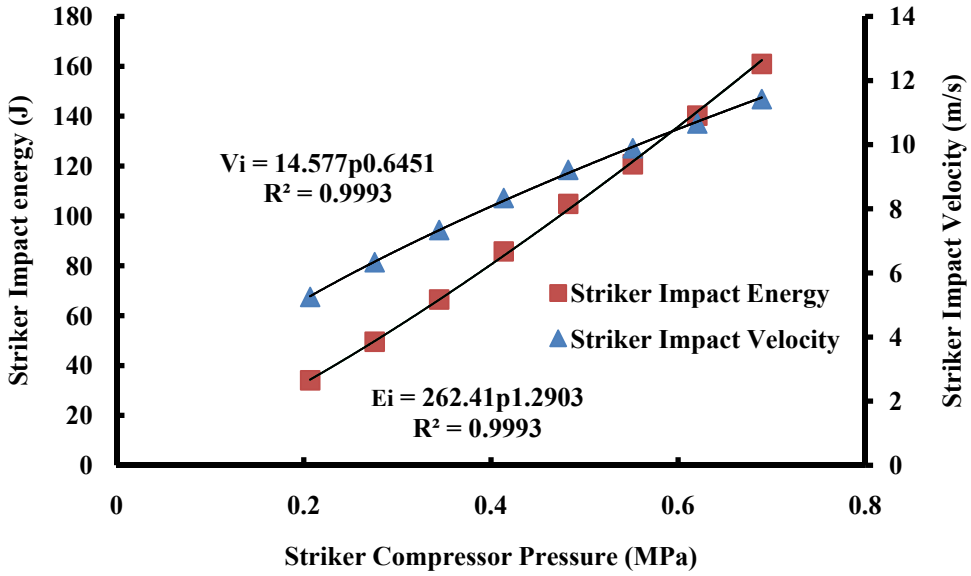

Figure 5. Relationship between the impact velocity, impact energy, and compressor pressure

ISSN 1927-0585 E-ISSN 1927-0593

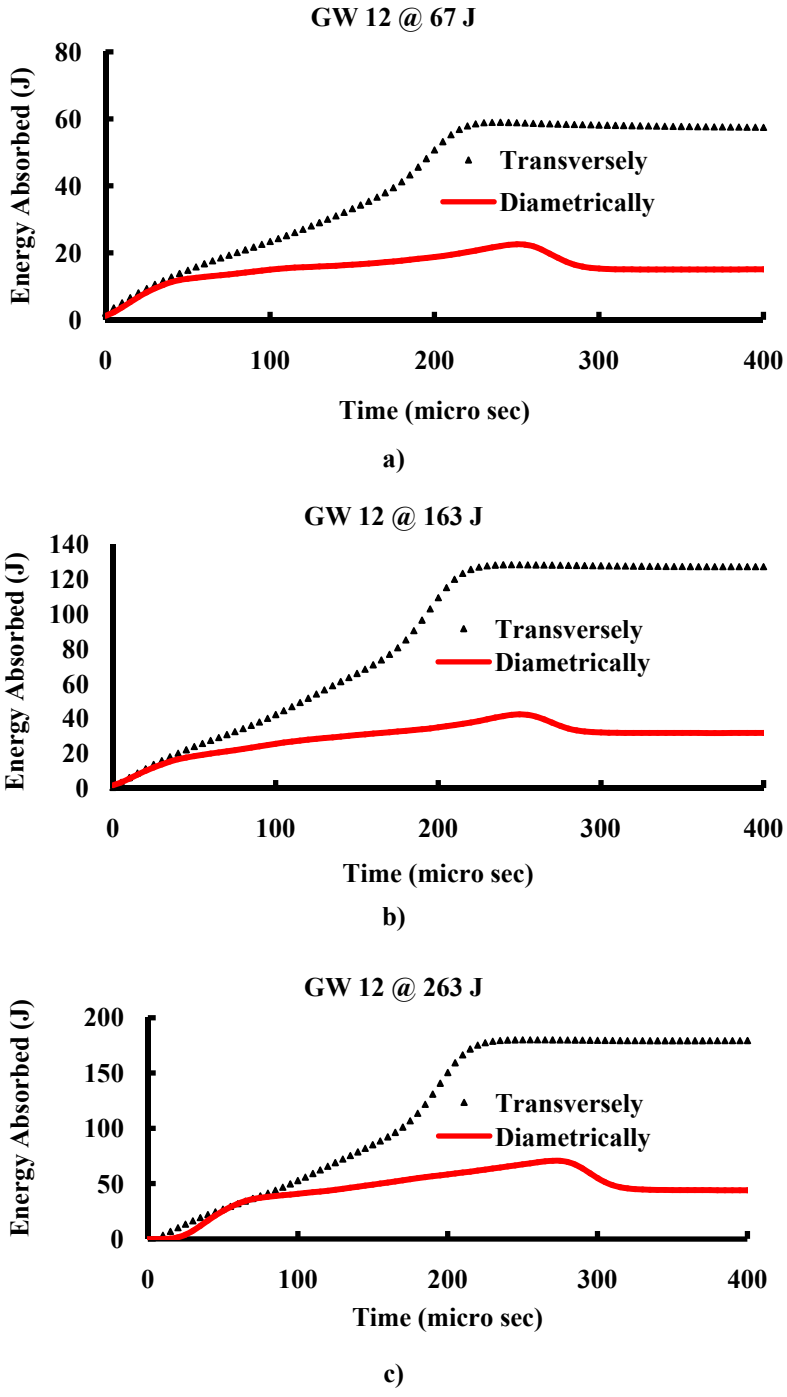

Figure 6. Effect of the loading direction on the energy absorbed for 12 layers specimens at the same impact energy of a) 67 J, b) 163 J, and c) 263 J

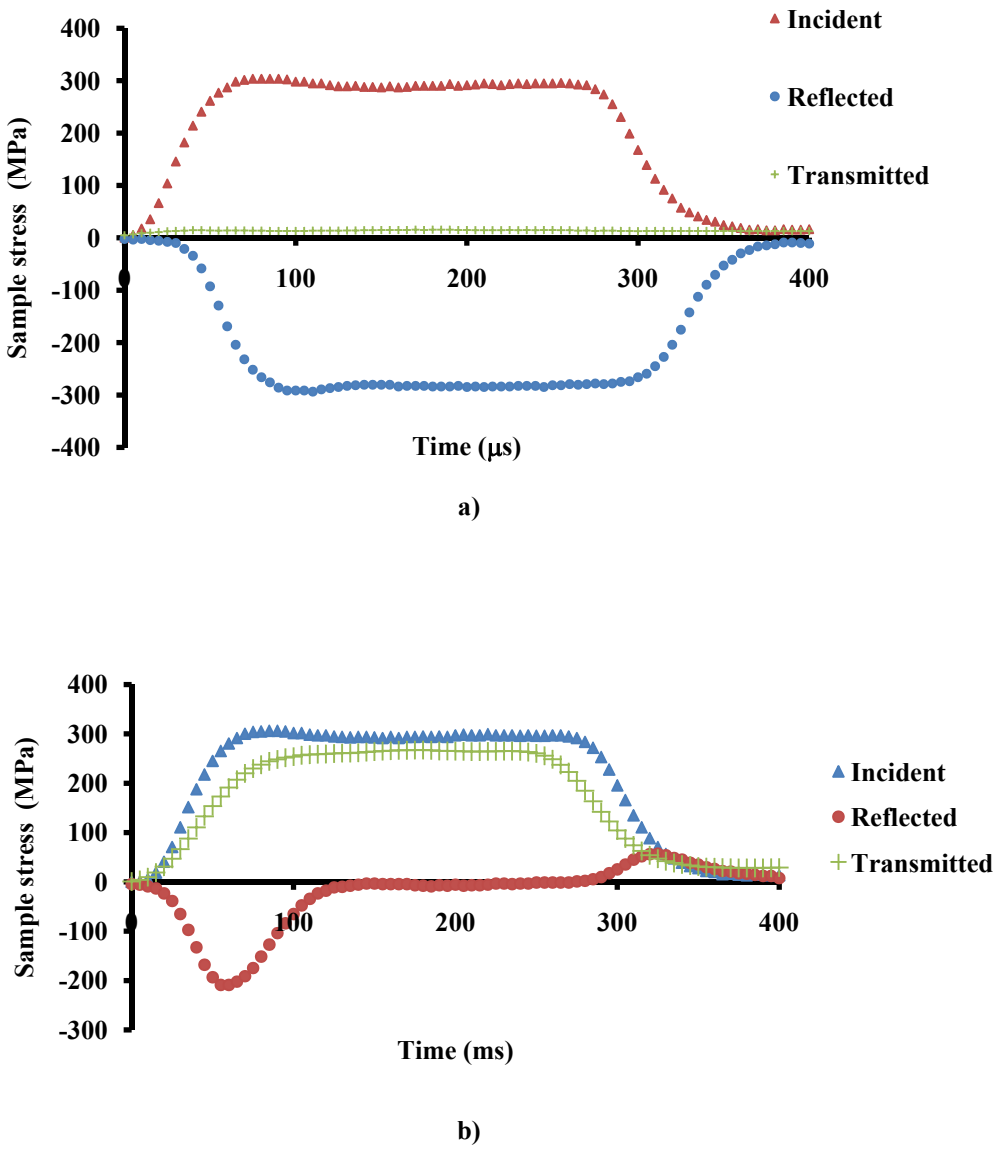

Figure 7. Incident, reflected, and transmitted stress waveforms for a) diametrical loading case and b) transverse loading case

ISSN 1927-0585 E-ISSN 1927-0593

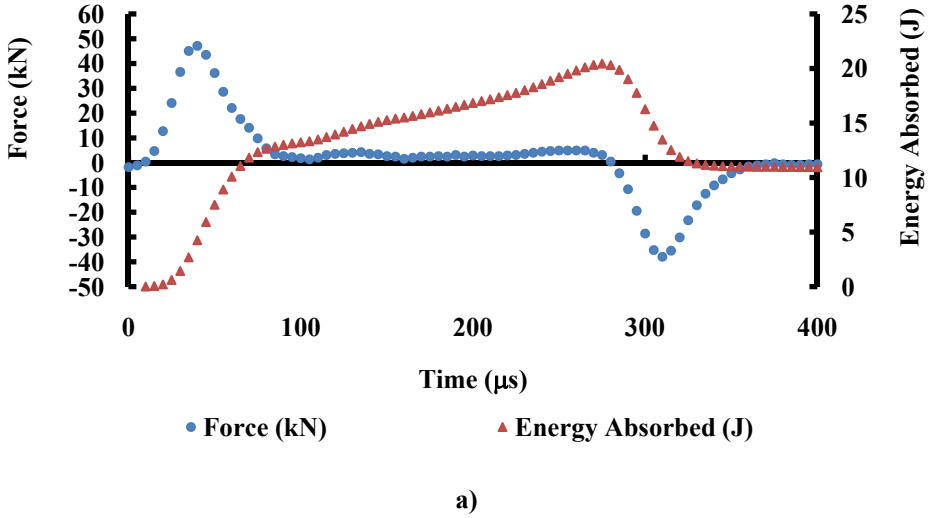

a)

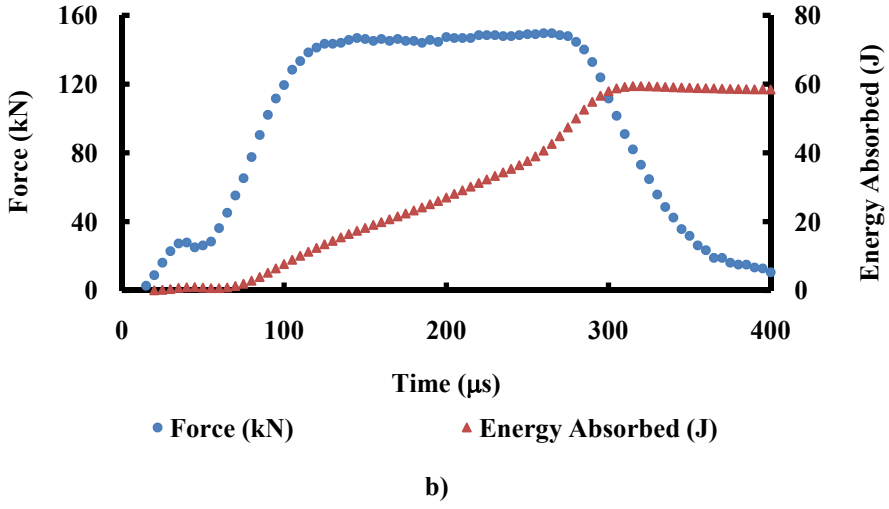

b)

Figure 8. The relationship between energy absorbed and applied force for a) diametrical loading case and b) transverse loading case

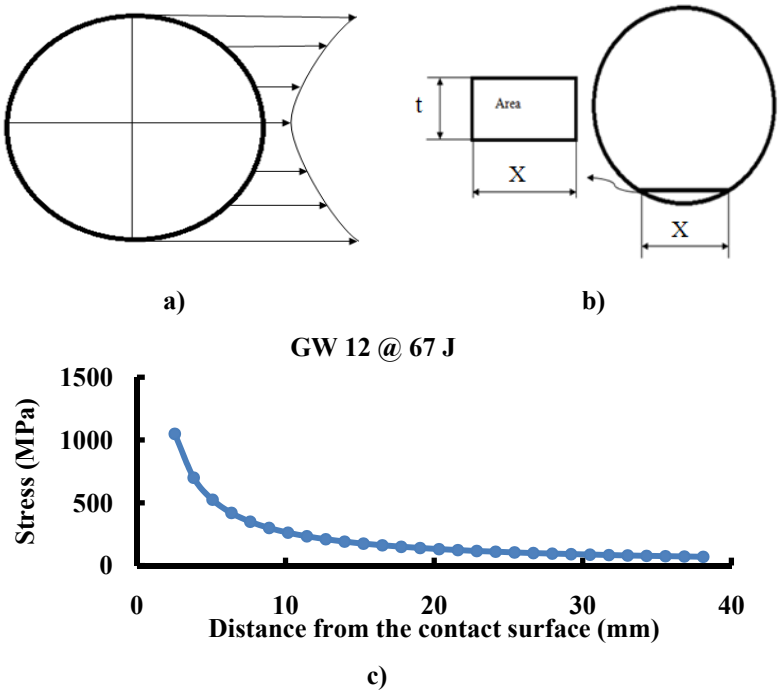

Figure 9. Schematic of a) stress concentration, b) unit area in the diametrically loaded specimens, and c) stress concentration in the specimen with respect to the distance from the contact surface

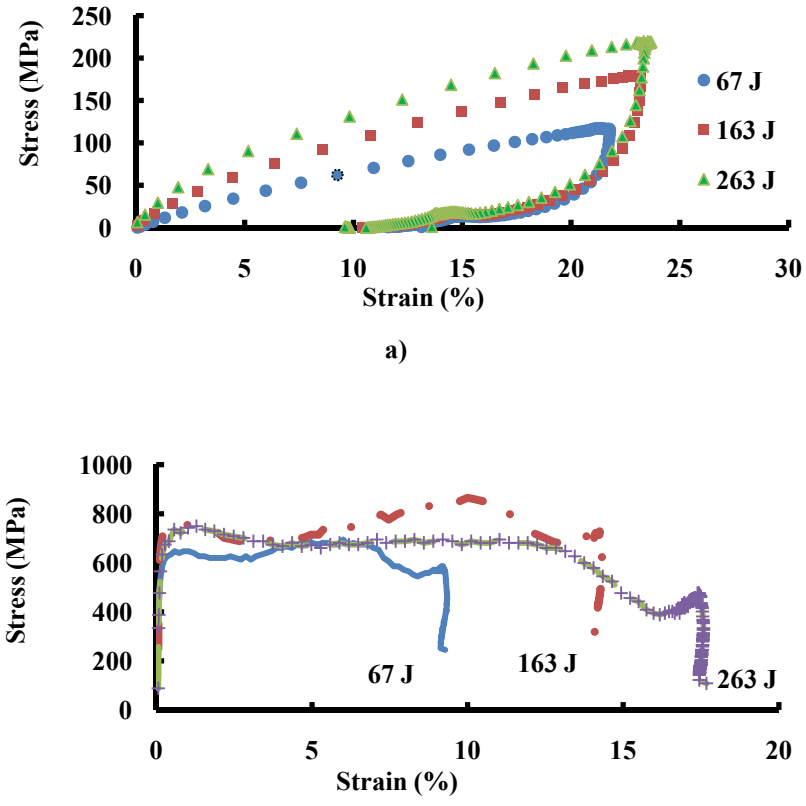

Figure 10. Stress - strain plot with varying impact energies of GW 12 specimens for a) transversely and b) diametrically loaded

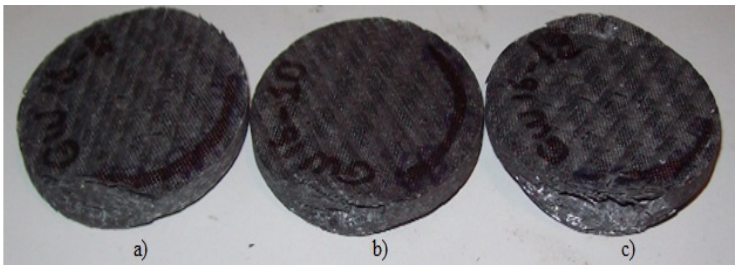

Figure 11. Diametrically loaded specimens at the applied impact energies of a) 67 J, b) 163 J, and c) 263 J

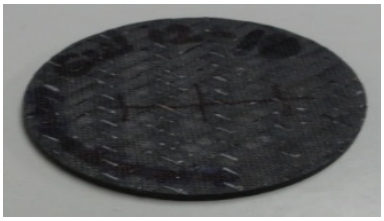

Figure 12. Representative transversely loaded specimen showing no visible damage at the highest impact energy of 263 J

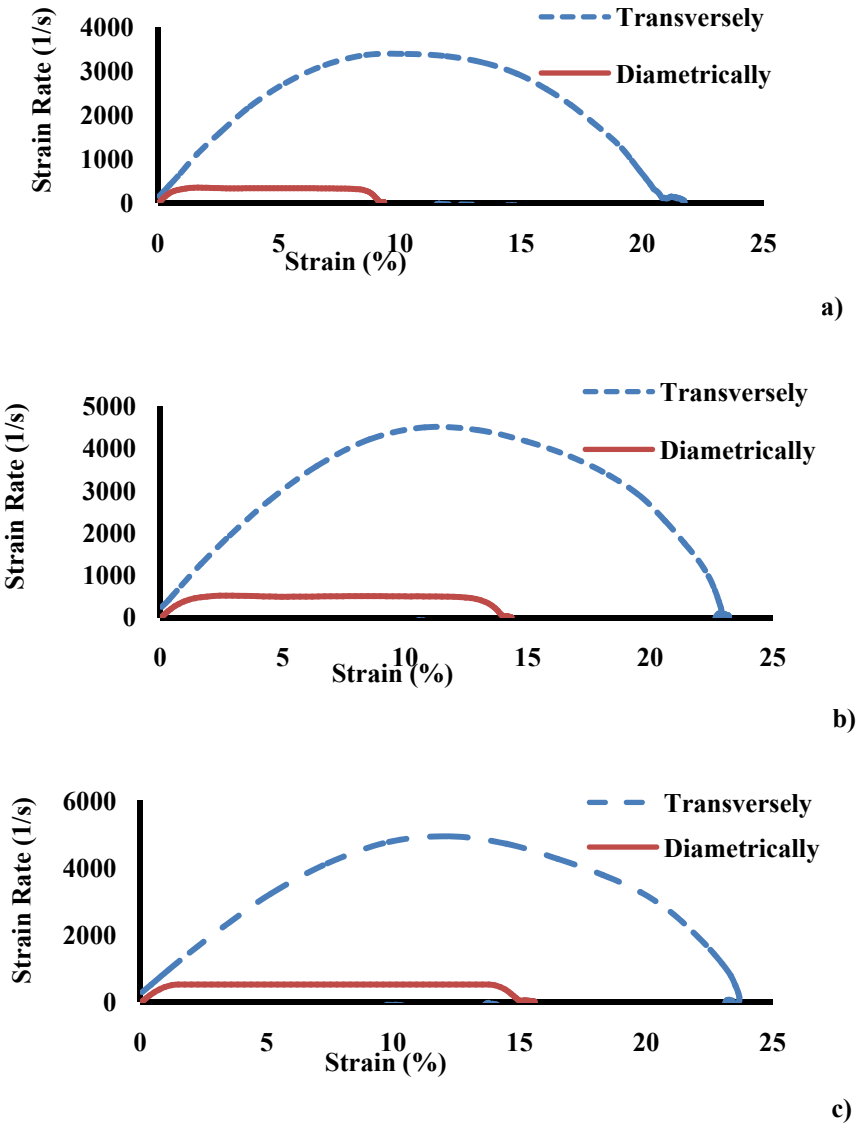

Figure 13. Effect of the loading direction on strain rate – strain behavior for 12 layers specimens at the same impact energy of a) 67 J, b) 163 J, and c) 263 J

ISSN 1927-0585 E-ISSN 1927-0593

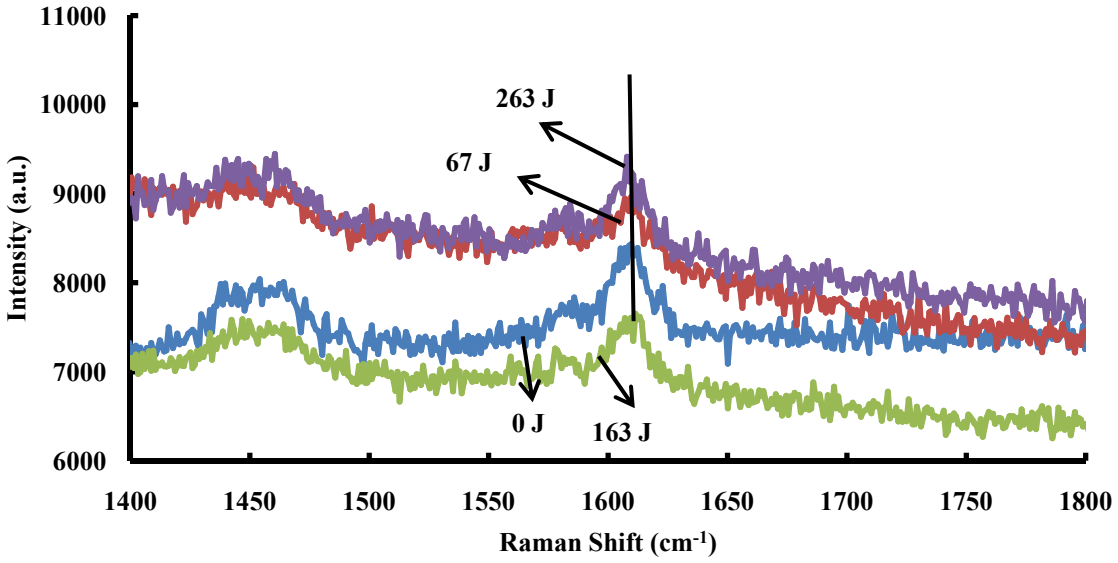

Figure 14. Raman spectrum of 16 ply (GW 16 specimen) transversely loaded specimen at various impact energies

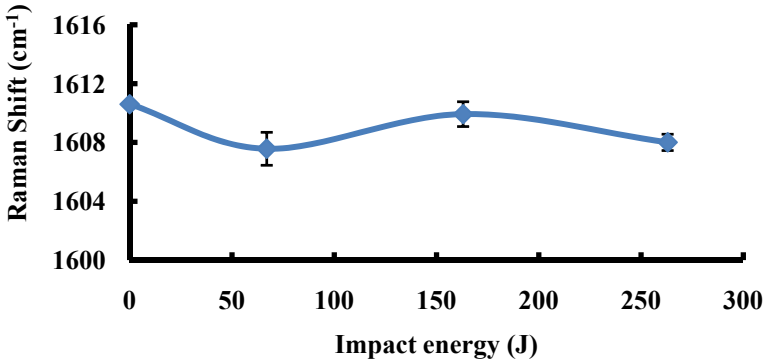

Figure 15. Relationship between the Raman Shift and impact energy for the 16 ply (GW 16 specimen) transversely loaded specimen

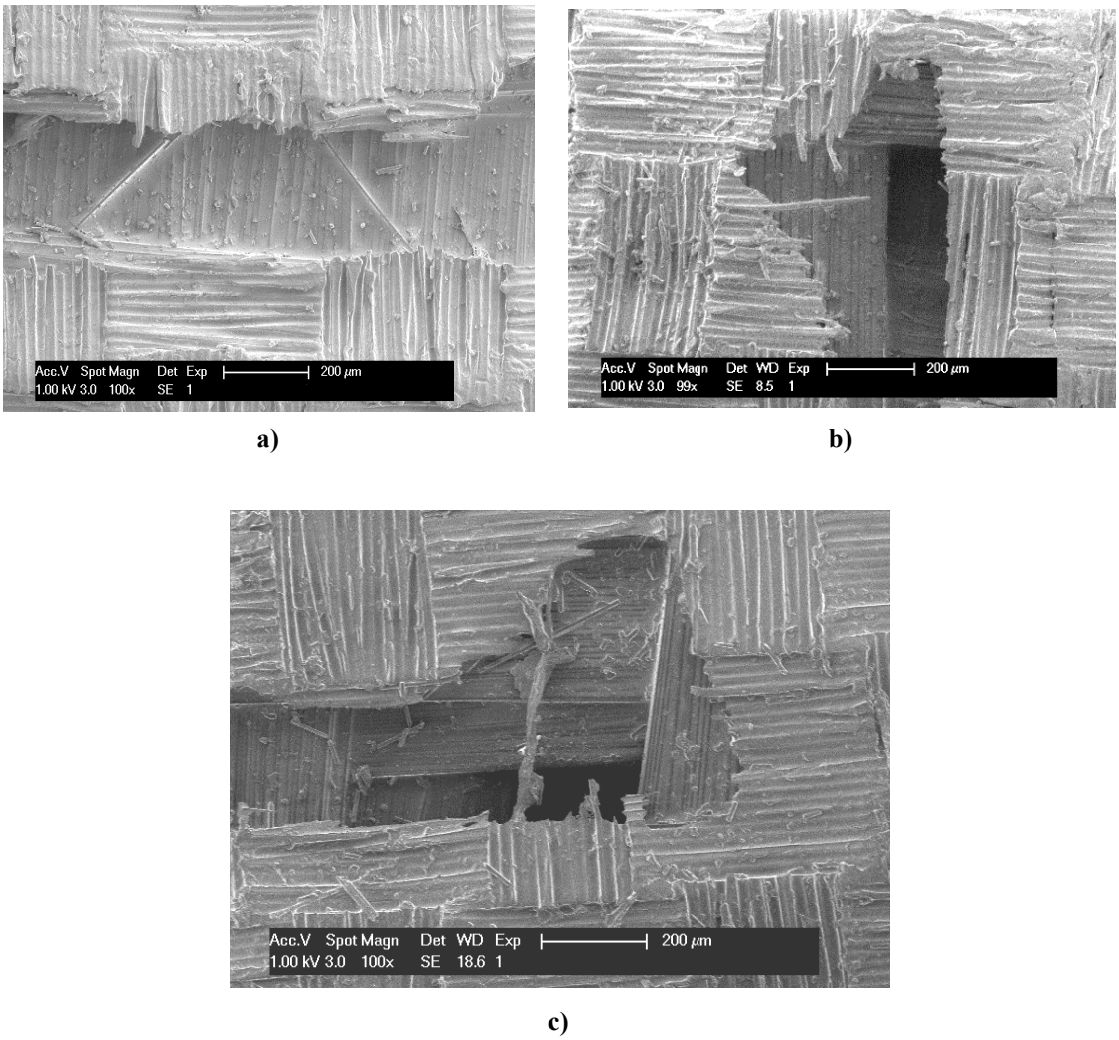

Figure 16. SEM images of transversely loaded specimens at a) 67 J, b) 163 J, and c) 263 J

 ISSN 1927-0585 E-ISSN 1927-0593

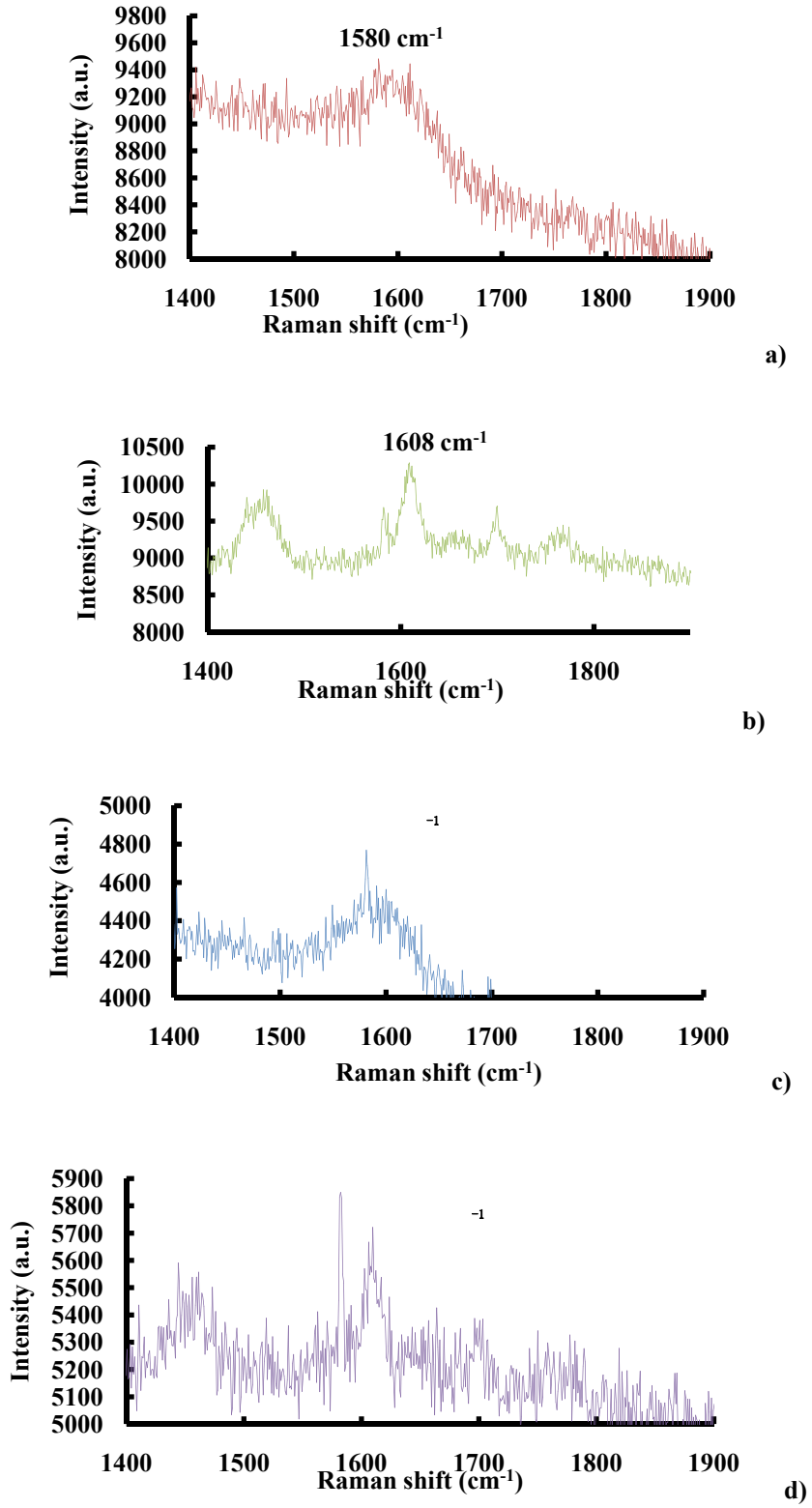

Figure 17. Raman spectrum of 16 ply diametrically loaded specimen at the impact energies of a) 0 J, b) 67 J, c) 163 J, and d) 263 J

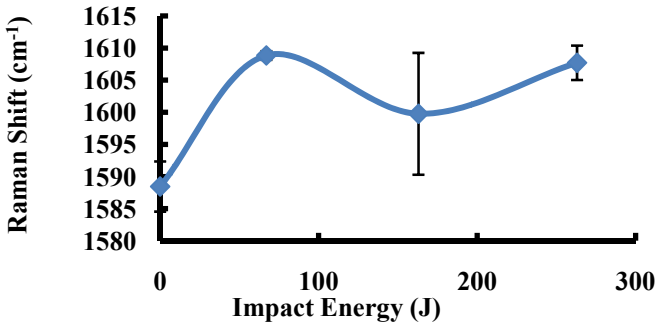

Figure 18. Relationship between the Raman Shift and impact energy for the 16 ply (GW specimen) diametrically loaded specimen

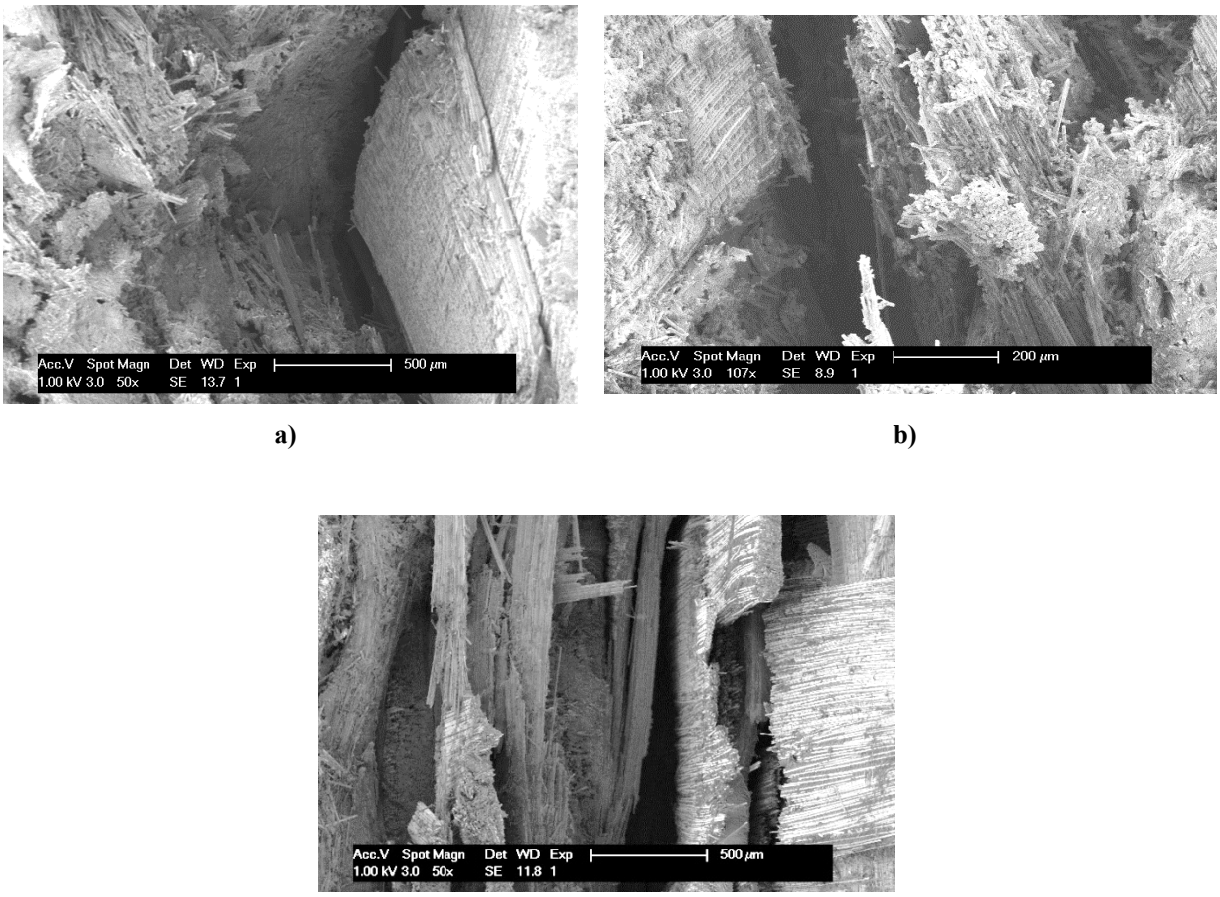

a) b)

c)

Figure 19. SEM images of diametrically loaded specimens at a) 67 J, b) 163 J, and c) 263 J

ISSN 1927-0585 E-ISSN 1927-0593